Nuclear Instruments and Methods in Physics Research B 539 (2023) 33–42

Contents lists available at ScienceDirect

Nuclear Inst. and Methods in Physics Research, B

journal homepage: www.elsevier.com/locate/nimb

Offline commissioning of a new gas cell for the MARA Low-Energy Branch ☆

A. Zadvornaya [a,*], J. Romero [a,c], T. Eronen [a], W. Gins [a], A. Kankainen [a], I.D. Moore [a], P. Papadakis [b], I. Pohjalainen [a], M. Reponen [a], S. Rinta-Antila [a], J. Sarén [a], D. Simonovski [d,e], J. Uusitalo [a]

[a] Accelerator Laboratory, Department of Physics, University of Jyväskylä, P.O. Box 35, 40014 Jyväskylä, Finland
[b] Nuclear Physics Group, STFC Daresbury Laboratory, Keckwick Lane, Warrington, Cheshire, WA4 4AD, United Kingdom
[c] Oliver Lodge Laboratory, University of Liverpool, Liverpool, L69 7ZE, United Kingdom
[d] Saint Petersburg State University, 7/9 Universitetskaya Emb., 199034, Saint Petersburg, Russian Federation
[e] Konstantinov Petersburg Nuclear Physics Institute (PNPI), National Research Center Kurchatov Institute, Gatchina, Leningradskaya Oblast, Russian Federation

ARTICLE INFO

Keywords:
Gas cell
MARA-LEB
^{223}Ra α-recoil source
In-gas laser ionization

ABSTRACT

Results of offline commissioning tests for a new dedicated gas cell for the Mass Analysing Recoil Apparatus (MARA) Low-Energy Branch are reported. Evacuation time, ion survival and transport efficiency in helium buffer gas were characterized with a radioactive ^{223}Ra α-recoil source. Suppression of the ion signal, originating from non-neutralized species in the gas cell, was explored with ^{219}Rn ions, the daughter recoil of ^{223}Ra, as a function of voltage applied to one of the ion-collector electrodes. Two-step laser resonance ionization of stable tin isotopes produced inside the gas cell from a heated bronze filament was demonstrated, and broadening of the atomic resonances in argon buffer gas was studied. These tests indicate the suitability of the new gas cell for future in-gas laser spectroscopy studies of exotic nuclei at the Accelerator Laboratory of the University of Jyväskylä.

1. Introduction

The MARA Low-Energy Branch (MARA-LEB) is a new low-energy radioactive ion beam facility under development at the Accelerator Laboratory of the University of Jyväskylä (JYFL-ACCLAB) for the study of exotic nuclei using high-resolution laser spectroscopy, mass measurements and nuclear decay spectroscopy [1]. MARA-LEB aims to provide a detailed understanding of exotic nuclear-structure phenomena by exploring several regions of the nuclear chart, including nuclei with $N \sim Z$ between Zr ($Z = 40$) and Sn ($Z = 50$), nuclei just above ^{100}Sn, as well as heavier, rare-earth proton dripline nuclei favored for extreme ground-state prolate deformation. Nuclei close to the $N = Z$ line provide a fertile landscape to explore nuclear phenomena including the effects of enhanced proton–neutron interactions and related pairing effects, long-lived isomeric states, exotic nuclear decays and the evolution of nuclear shapes and sizes. Additionally, the astrophysical rapid proton capture (rp) process [2] and the νp process [3] traverse through this region. The isotopic selectivity of MARA-LEB, in combination with a planned high-efficiency decay station, will offer opportunities for nuclear decay spectroscopy of rare-earth nuclei ($57 \leq Z \leq 71$), in particular the study of proton decay fine structure and nuclear shapes. More recently, multi-nucleon transfer reaction studies at the MARA vacuum-mode recoil separator have been performed, and reaction products of light actinide isotopes have been identified and their production cross sections measured [4]. Depending on the available primary beam intensities and experimental efficiencies, optical spectroscopy of actinide isotopes may be feasible at the new facility.

The first phase of MARA-LEB is under construction, with all major parts of the setup being manufactured [1,5]. Stable primary beams from the K130 heavy-ion cyclotron are delivered to MARA with intensities of at least 200 pnA, impinging on thin foil targets mounted on a rotating wheel at the target position of the separator. Recoiling ions with a variety of mass-to-charge ratios are separated with a combination of static electric and magnetic fields. Depending on the reaction symmetry, two to six charge states corresponding to the mass of interest are transported to the focal plane detection system [6]. MARA has a mass resolving power of roughly 250, and uses sets of movable mechanical slits to improve this value at a cost of acceptance. For the operation of MARA-LEB, a gas cell will be located at the focal plane. From the original charge-state distribution, one to three charge states can be accepted through the gas-cell window. In this manner, mass-selected recoil ions of interest, e.g., ^{94}Ag or ^{102}Sn with an energy of about 200 MeV

☆ The results presented in this paper are based on work performed before Feb 24th 2022.

* Correspondence to: II. Physikalisches Institut, Justus-Liebig-Universität Gießen, 35392 Gießen, Germany.
E-mail address: Alexandra.Zadvornaya@exp2.physik.uni-giessen.de (A. Zadvornaya).

https://doi.org/10.1016/j.nimb.2023.03.016
Received 29 May 2022; Received in revised form 12 February 2023; Accepted 16 March 2023
Available online 24 March 2023

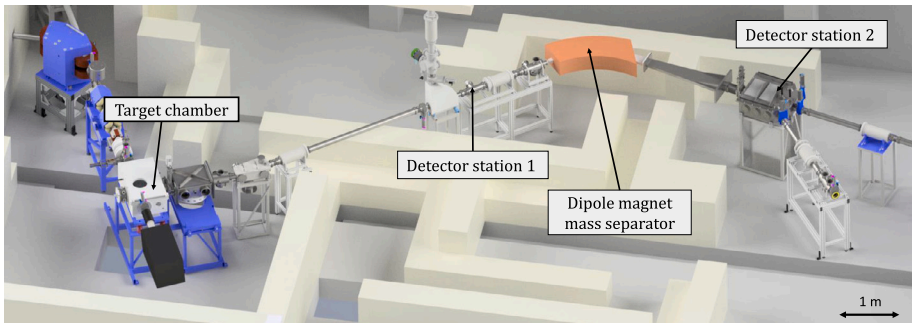

Fig. 1. A simplified three-dimensional overview of the parts of the IGISOL facility relevant to this work. The gas cell, not visible in this overview, was housed in the target chamber. The dipole magnet for mass separation and detector stations 1 (silicon detector) and 2 (silicon and MCP detectors) are denoted.

and yields of a few ions/s, will be stopped and thermalized in either argon or helium. In the case of argon, ions will be neutralized, allowing for subsequent selective resonance laser ionization and spectroscopy of elements of interest either via in-gas cell or in-gas jet configurations, similar to the approach described in [7]. Helium on the other hand is less conducive to neutralization, and thus ions have a higher survival probability. Nevertheless, shorter evacuation times can be achieved in helium, giving access to the study of nuclei with shorter half-lives that do not require laser re-ionization. After extraction from either helium or argon gas, ions will be re-accelerated to 30 keV towards the low-energy branch for downstream experiments.

A prototype gas cell has been designed at the In-Gas Laser Ionization and Spectroscopy (IGLIS) laboratory of KU Leuven (Belgium) for future use at the online Rare Element in Gas Laser Ion source and Spectroscopy (REGLIS^3) facility at S^3 GANIL (France) [8]. COMSOL Multiphysics software [9] was used to optimize the gas-cell geometry in order to minimize the diffusion losses and the transport time of ions extracted through the gas cell [8]. Studies have shown that to overcome the effect of collisional- and temperature-broadening mechanisms to the atomic line spectral resolution, resonance ionization spectroscopy must be performed in the low-density and low-temperature medium of a supersonic gas flow rather than in the subsonic flow inside the gas cell [10]. Formation of uniform and spatially extended gas jets is essential for high efficiency and high resolution of the in-gas jet method, and can be achieved with carefully designed and manufactured de Laval nozzles of high Mach numbers, M [11].

In this work, we present an overview and results from commissioning tests of a new gas cell for MARA-LEB, the design of which is similar to the gas cell planned for the S^3 facility, GANIL. These tests were performed at the Ion Guide Isotope Separator On-Line (IGISOL) facility [12] which is briefly described in Section 2. A radioactive ^{223}Ra α-recoil source [13] was installed inside the gas cell. The evacuation time, ion survival and transport efficiency were characterized using the daughter ^{219}Rn recoil ions stopped in helium buffer gas, discussed in Section 3. These tests were followed by in-gas cell laser ionization of stable tin isotopes, this time in an argon buffer-gas environment (Section 4). The latter work is in anticipation of one part of the planned science program of the MARA-LEB facility, aiming to study the ground-state electromagnetic moments and mean-squared charge radii for neutron-deficient tin isotopes. Such information is not yet available for isotopes with neutron number $N < 58$ [14]. We note that in-gas laser ionization of stable tin isotopes has earlier been demonstrated at the LISOL facility as part of the preparatory experiments towards REGLIS^3 at S^3 GANIL [7]. Our conclusions are presented in Section 5.

2. Experimental method

2.1. IGISOL facility

Commissioning tests with the MARA-LEB gas cell were carried out at the IGISOL facility at the University of Jyväskylä. Fig. 1 highlights the relevant parts of the facility used in this work. The MARA-LEB gas cell was installed in the target chamber of the facility. Isotopes of interest were produced and stopped in the gas cell filled with high-purity helium or argon gas and transported by the gas flow towards the free jet nozzle and into a sextupole ion guide (SPIG) [15]. The recombination rate coefficient of argon ions in neutral argon gas is an order of magnitude larger than that for helium [16,17]. For this reason, argon is favored as the buffer gas of choice when performing selective resonant laser re-ionization under online conditions as the larger recombination rate leads to a higher probability of neutralization [18]. It is important to note, only high-purity gases were used in the following tests. Purification of helium was achieved with liquid nitrogen-cooled cold traps, while for argon, a getter purifier was used (Saes MonoTor PS4-MT15) as described in detail in Ref. [19]. Subsequently, after guidance through the SPIG, the ions were accelerated to 30 keV and transported towards a magnetic dipole mass separator having a mass resolving power $M/\Delta M$ of about 500.

Two detector stations were used in the commissioning tests, as shown in Fig. 1. Detector station 1, located before the mass separator, consists of a silicon detector and was used to determine ion survival and transport efficiency by measuring the number of implanted ions identified via their radioactive (alpha) decays. Detector station 2 is located in the focal plane area of the separator, within the so-called electrostatic switchyard, and consists of a silicon detector and a microchannel plate (MCP) detector. The MCP detector is used when mass scans are performed, and to determine the evacuation time of mass-separated ions extracted from the gas cell as it allows for time-resolved ion counting. Similar to Detector station 1, the silicon detector after the mass separator can be used to determine the ion survival and transport efficiency of radioactive ions, but cannot be used for stable beams.

A two-step resonant laser ionization scheme for tin was realized using solid-state lasers from the Fast Universal Resonant laser IOn Source (FURIOS) laboratory [20]. The Titanium:sapphire (Ti:Sa) laser resonators, pumped by 10-kHz repetition rate Nd:YAG lasers, are either in-house built or sourced from Johannes Gutenberg University Mainz. The FURIOS laboratory, located directly above the target chamber on the second floor of the facility, houses two pump lasers, model Lee Laser LDP-200, with a nominal output power of about 100 W at 532 nm with 100 ns temporal pulse width. Each Ti:Sa laser is pumped with 10–25 W, split from the main pump beam using half-wave plates and polarizing beam splitter cubes. The Ti:Sa lasers are either in Z-shaped or bowtie cavity configurations, with the latter providing narrowband operation via injection-locking techniques [21]. In this work, only the broadband Z-shaped resonators are used. The lasers are equipped with intra-cavity second harmonic generation capability and have access to external harmonic generation setups enabling a wavelength tunability from about 210–500 nm and 690–1000 nm.

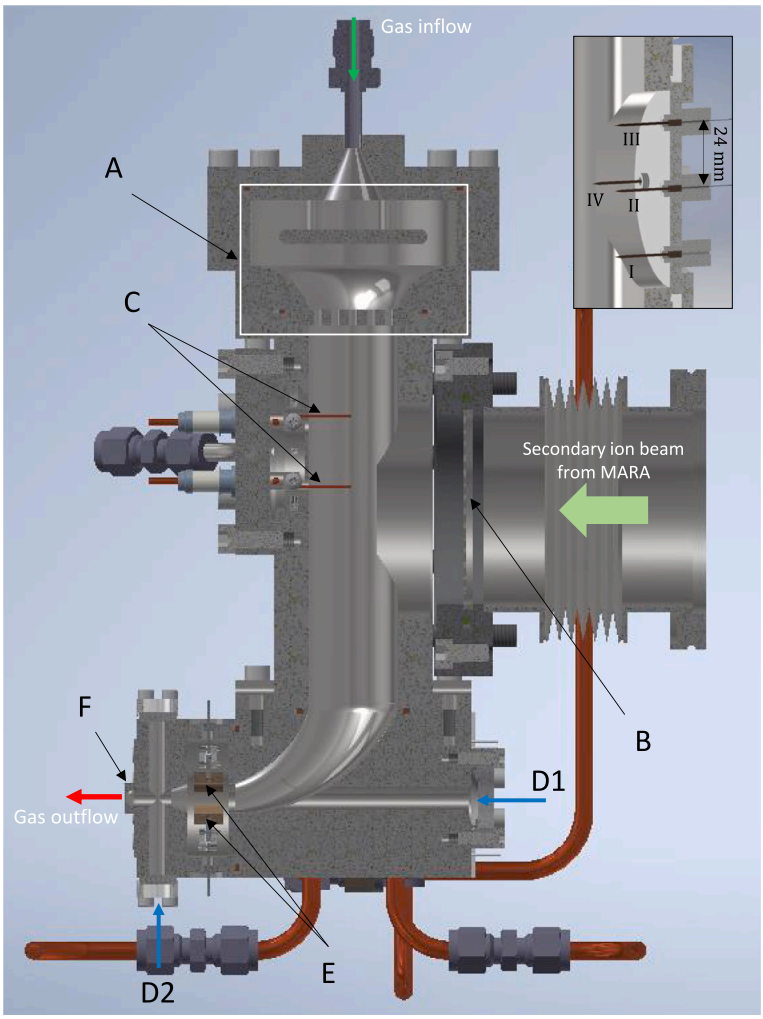

Fig. 2. Cutaway view of the MARA-LEB gas cell. Gas inflow and outflow are indicated with green and red arrows, respectively. The mass-selected secondary ion beam from the MARA separator is denoted with a light green arrow. A — pre-chamber for gas-flow conditioning (houses obstacle and honeycomb flanges), B — entrance window (foil window), C — filament feedthroughs, D1 and D2 — laser viewports for collinear and transverse resonant laser ionization configurations, respectively, E — ion-collector electrodes, F — free jet/de Laval nozzle. The entrance window can be replaced by a flange to which a ^{223}Ra α-recoil source can be mounted in different positions as shown in the inset on the upper right.

2.2. MARA-LEB gas cell

The geometry of the MARA-LEB gas cell is based on the design to be used for the REGLIS^3 facility, S^3 GANIL [8]. A cutaway view of the gas cell is shown in Fig. 2. A number of modifications have been implemented, including an increase in the diameter of the entrance window through which the recoil products from the MARA separator must pass, and the location of the flange housing two filament feedthroughs, which has been moved from the central axis of the separator. Three individual operational modes are feasible:

- Online mode: the ions from the MARA separator will enter the gas cell through a thin foil window, typically havar or mylar with a thickness up to ~10 μm and an open diameter of 64 mm. The window is supported by a honeycomb frame. Recoils are thermalized and stopped in a high-purity gas.
- Offline mode with α-recoil source: the foil window can be replaced by a flange to which a ^{223}Ra α-recoil source is mounted, as shown in the inset in Fig. 2.
- Offline mode with filaments containing stable (or long-lived) isotopes of interest: two filaments can be mounted on a flange, offset and opposite to the entrance window. Through resistive heating, a continuous source of atoms is produced (in this work, a bronze filament is used to produce stable tin isotopes).

In this work, the MARA-LEB gas cell was operated only in the aforementioned offline modes. Ion-collector electrodes (ICs) installed before the free jet nozzle of the gas cell are used to collect non-neutralized ions transported from the stopping region, thereby increasing the selectivity when in-gas cell/in-gas jet laser ionization is used under online conditions. Stopping and laser ionization volumes are physically separated in order to reduce the effects of recombination of photo-ions. This allows for more efficient low-resolution in-gas cell resonance ionization spectroscopy (RIS). In-gas laser ionization can be implemented in collinear, transverse or crossed-beam geometries with respect to the atom flow via laser viewports D1 and D2 (see Fig. 2). Finally, isotopes of interest and the buffer gas atoms leave the gas cell via a free jet or de Laval nozzle, the latter employed to form collimated high Mach number gas jets. In this work, a free jet nozzle with a diameter of 1.65 mm was used.

3. Offline tests with a ^{223}Ra α-recoil source

Combined efficiency of ion survival and transport, as well as evacuation time from the gas cell are important parameters characterizing gas-cell performance. These parameters have been studied in this work with a radioactive ^{223}Ra α-recoil source, installed inside the gas cell operated using helium buffer gas. Fig. 3 shows the gas cell mounted inside the target chamber of the IGISOL facility. Prior to the tests, ^{223}Ra ions ($T_{1/2}$ = 11.4 d) were accumulated on the tip of a needle

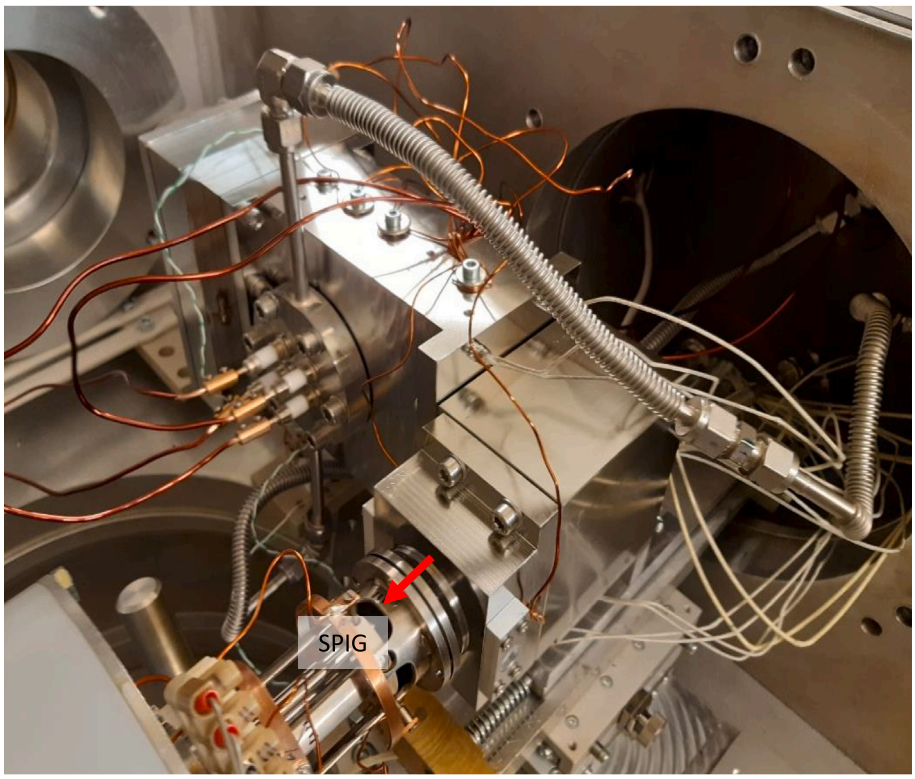

Fig. 3. MARA-LEB gas cell installed in the target chamber of the IGISOL facility during the commissioning tests. The free jet nozzle cannot be seen due to its close distance, ~2 mm, to the SPIG electrode (labeled in the photograph). Gas outflow is indicated with a red arrow.

(the "needle source") installed in an α-recoil generator, with ^{227}Ac ($T_{1/2}$ = 21.8 y) used as the primary source. An accumulated activity of (4.0 ± 0.4) kBq of ^{223}Ra was measured in a separate vacuum chamber before installing the needle into the gas cell. During the following tests, performed over several consecutive days, the source was installed in four positions as shown in the inset in Fig. 2. For each position, α-recoil spectra of ^{219}Rn ions, the daughter product of ^{223}Ra with a half-life of 3.96 s, were recorded at Detector station 1 for different values of pressure P_0 inside the gas cell. An example spectrum is shown in Fig. 4 for the source in position I and helium pressure P_0 of 300 mbar. During these measurements, only 50% of the ^{219}Rn ions were released into the buffer gas due to the source geometry at a rate of about 1300 ions/s. The measured counting rate at Detector station 1 for this source position was 160 counts/s. Analysis of the accumulated spectra was performed in a manner similar to that described in [22], and the efficiency of ion survival and transport to the detector station was extracted. We note that helium was chosen as the buffer gas due to the smaller recombination rate coefficient compared to that of argon. We could therefore anticipate higher counting rates of the detected recoil ions. Indeed, such comparisons have been studied at the IGISOL facility in the past and support this choice of gas for ion survival.

To determine the evacuation time for different starting coordinates inside the gas cell, voltage pulses were applied to the needle. The source was connected to a power supply, the output voltage of which could be programmed by using TTL logic. During a recording cycle, lasting 0.67 s for helium and 1.34 s for argon, the voltage at the needle was maintained at −30 V, except for short periods of 50 ms or 150 ms (for helium and argon, respectively) when the voltage was set to 0 V, thus allowing the release of ^{219}Rn ions into the gas flow. Time profiles of singly-charged ions extracted from the gas cell were subsequently recorded using a multi-channel scaler (MCS) for time-resolved counting of the ion signal from the MCP detector at Detector station 2, located in the electrostatic switchyard as shown in Fig. 1. A timing card was used to provide the trigger for the MCS to start recording and to change the voltage at the needle source. To improve the signal-to-noise ratio, time profiles were accumulated over a number of recording cycles.

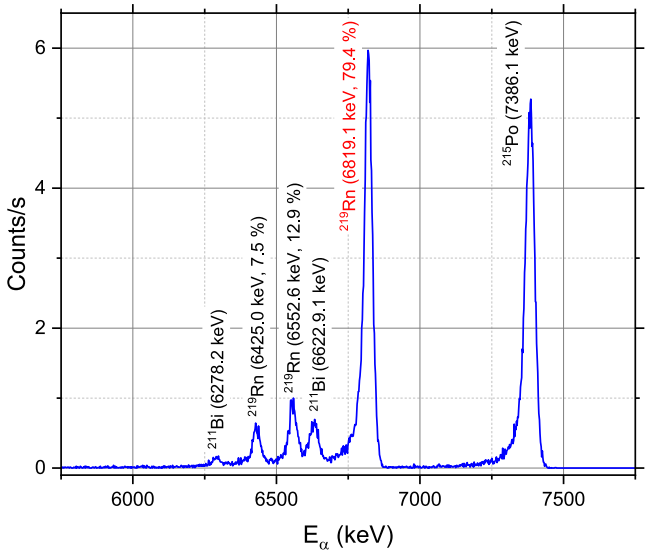

Fig. 4. Example of an α-decay spectrum of ^{219}Rn measured at Detector station 1 for the needle source in position I and a helium pressure P_0 of 300 mbar. The ^{219}Rn peak used for extracting the efficiency is denoted in red. The peaks are labeled according to the alpha decay from the respective isotope, energy of the alpha particle and, for ^{219}Rn, the branching ratio.

3.1. Ion survival and transport efficiency

The ion survival and transport efficiency was measured for all positions of the needle source as a function of helium gas pressure P_0 up

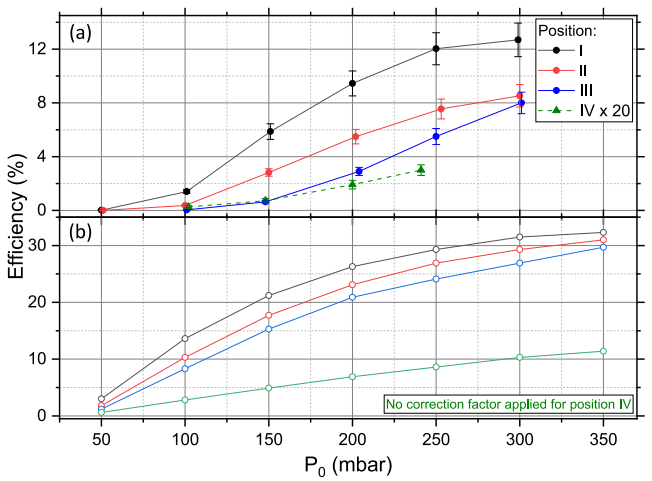

Fig. 5. Efficiency for the needle source in positions I, II, III and IV at different values of helium pressure P_0. (a) Ion survival and transport efficiency measured at Detector station 1. The results for position IV are multiplied by a factor of 20. (b) Numerical calculations of the efficiency of ion survival against diffusion losses.

to 300 mbar, limited by the pressure in the surrounding IGISOL target chamber. We note that this limitation will be mitigated at MARA-LEB due to the anticipated use of a nozzle with a smaller diameter of 1 mm and, therefore, smaller flow rate, for which the pumping capacity for MARA-LEB has been tailored accordingly. Moving the needle source to a new position required venting of the target chamber, thus potentially exposing the gas cell to the ambient air. This could detrimentally affect the efficiency via potential losses of charged recoils to molecular adducts. For this reason, after measuring at every needle position the gas cell was baked overnight using cartridge heaters ($T \approx 100°C$) and subsequently cooled to room temperature with a small flow of helium ($P_0 \approx 50$ mbar). The efficiency is shown in Fig. 5(a). As the measurements were performed using Detector station 1 there is no separation of different mass-to-charge (m/q) values, nor identification of potential molecular ions. However, Detector station 2 was also used to verify that no higher charged states or heavier molecular ions were present in the extracted beam. A maximum efficiency of (12.7 ± 1.3) % was measured for the source in position I for a pressure P_0 of 300 mbar. We note that this efficiency includes the transport efficiency from the exit of the gas cell to the detector station, in addition to the extraction through the helium gas. The tip of the needle was unfortunately scratched on the gas-cell surface while moving it from position II to position III, resulting in a loss of activity compared with what would be expected from the half-life alone (this was confirmed after the gas-cell measurements). The results shown in Fig. 5(a) for positions III and IV have therefore been corrected for this reduction factor of 2.9. Moreover, the results for position IV in Fig. 5(a) are multiplied by a factor of 20, for better readability of the measured data.

Numerical calculations were performed using the Computational Fluid Dynamics (CFD) module of COMSOL Multiphysics software [9]. The velocity of the gas flow inside the gas cell depends on the cross-sectional area of the gas outflow and therefore the diameter of the available free jet nozzle was accurately measured to be (1.65±0.07) mm. The output of the numerical calculations for the velocity of the helium gas flow and its streamlines is shown in Fig. 6. The calculations only include the diffusion losses of the simulated atoms to the inner walls of the gas cell. The losses are defined by the outflow diameter, the geometry of the gas cell, and the diffusion coefficient of the simulated atoms in the buffer gas. Due to the absence of a diffusion coefficient for radon in the literature, the coefficient for mercury ($A \sim 200$) in helium at normal conditions (273.15 K and 1013 mbar) was used as a Ref. [23], $D_{ref} = 5.32 \times 10^{-5}$ m^2/s, and scaled to the value of the helium pressure P_0. No significant influence on the calculated diffusion losses is expected. Results of the numerical calculations for the transport efficiency in the gas are shown in Fig. 5(b).

The notable difference between the absolute values of the measured and numerically calculated efficiency is anticipated. One factor that may contribute is that ion losses in the gas cell are determined not only by diffusion, but also by the presence of impurities in the buffer gas. Potential losses due to molecular formation were not considered in the simulation, but are expected to be present in the gas, albeit at significantly reduced amounts after the gas-cell baking. Impurities are also involved in other ion-loss mechanisms e.g., neutralization of ions via three-body recombination involving a free electron, dissociative recombination and charge-exchange reactions [24]. It has been shown that an ion survival and transport efficiency of up to 30 % can be reached for ^{219}Rn ions in gas cells operating with cryogenic helium at temperatures below 90 K [25,26]. This is due to the ultra-pure conditions attained by freezing out the impurities. Moreover, the efficiency depends on the chemical nature of the elements and therefore will be different for ^{219}Rn ions in, for example, helium and argon gas. A second factor is the transport efficiency from the gas cell to the silicon detector that depends on the tuning of the SPIG and mass separator. The simulations only include the transport through the gas cell.

Despite the discrepancy in the absolute values, it is encouraging to see that the general trend of the efficiency growth as a function of helium pressure is reproduced rather well, in particular for needle source positions I and II, for which the simulations and measurements show a similar saturation above 250 mbar. In addition, the relative efficiencies between the source locations are in agreement with experiment, i.e. the highest efficiency is obtained for position I and the lowest for position IV. The simulated efficiency of the latter position is most discrepant with the experimental values, perhaps indicating both an underestimated loss due to diffusion towards the walls of the gas cell, or other loss mechanisms not accounted for in the simulation and amplified in regions of slower gas flow close to position IV.

3.2. Evacuation time

Evacuation time profiles of ^{219}Rn$^+$, ^{20}Ne$^+$ and ^{40}Ar$^+$ ions extracted from the gas cell were recorded and analyzed for all positions of the needle source with the MCP detector at Detector station 2. In these measurements, argon and in-house recycled helium buffer gases were used. The helium included neon as an impurity, not present in the commercially bought argon [19]. Measurements were performed with a pressure P_0 of about 200 and 100 mbar in the cases of helium and argon gas, respectively, with the results shown in Fig. 7. Time profiles were fitted using the built-in Extreme Peak function from OriginPro software [27], which allowed the extraction of the peak centroid t_{max} and its full width at half maximum Δt, highlighted in Fig. 7, as well as the corresponding error bars. The fitting results, shown in Fig. 8, were then compared with a more sophisticated function analytically derived for the evacuation time by solving the diffusion–convection equations [28] and were found to be in good agreement within error bars, justifying therefore the use of a simpler function. The error bars of the peak centroids, as well of the widths in helium, are smaller than the data points shown in Fig. 8.

A higher signal-to-noise ratio was achieved for the ^{20}Ne$^+$ time profiles accumulated over a fewer number of recording cycles compared to ^{219}Rn$^+$. The extracted peak centroids of ^{219}Rn$^+$ and ^{20}Ne$^+$ ions are in agreement for the needle source in positions I and II and have a difference of less than 10 % for the needle source in position III. The evacuation time profile of ^{219}Rn$^+$ for the needle source in position IV was not recorded due to insufficient statistics. Moreover, peak centroids of ^{219}Rn$^+$ and ^{40}Ar$^+$ ions are in agreement for the measurements performed with argon buffer gas. This leads to the conclusion that ionization of buffer gas and its impurities (^{20}Ne$^+$, in case of helium buffer gas) takes place within a couple of mm around the needle tip by

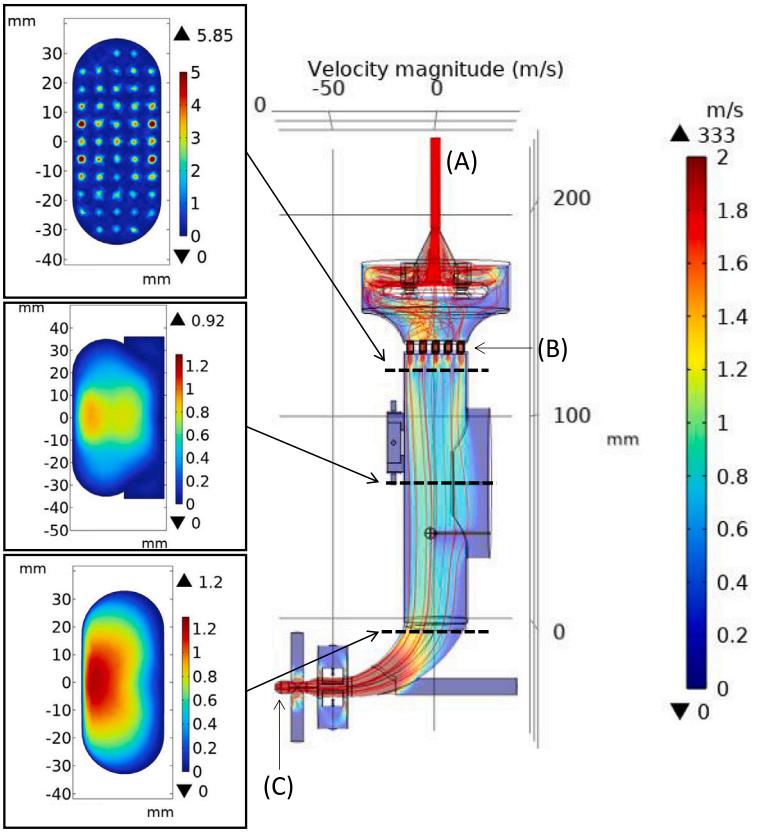

Fig. 6. Output of the numerical calculations of the velocity and flow streamlines inside the MARA-LEB gas cell. The color bar indicates the velocity magnitude with the upper limit set to 2 m/s to allow visualization of a slower gas flow in the central part of the gas cell. The gas inlet (A) is denoted. The effect of the honeycomb structure (B) used to achieve a uniform flow condition is clearly visible. The ions exit the gas cell at position (C). Velocity profile maps from different cross-sections of the gas cell are shown at the corresponding locations.

the $^{219}Rn^{+}$ ions, released in the decay of ^{223}Ra with an energy of about 104 keV. On the other hand, the alpha particles released with an energy of 5.7 MeV, deposit only about 30 keV per 1 cm traveled in 200 mbar helium buffer gas. Therefore, for the cases when the extracted ion signal of $^{219}Rn^{+}$ is too small, evacuation time profiles of ions of buffer gas and/or of its impurities can be used to estimate the evacuation time. Full widths at half-maximum of lighter $^{20}Ne^{+}$ and $^{40}Ar^{+}$ ions are larger compared to those of $^{219}Rn^{+}$, which can be explained by a larger diffusion coefficient.

The needle source positions I, II and III are separated by 24 mm, as indicated in the inset in Fig. 2. The corresponding peak centroids for $^{20}Ne^{+}$ ions are delayed by approximately 27 ms for each subsequent position, allowing the velocity of the helium gas to be estimated as 0.9 m/s in that section of the gas cell, in good agreement with numerical calculations of the velocity shown in Fig. 6. Moreover, peak centroids of $^{20}Ne^{+}$ coincide for the source in positions II and IV, thus illustrating that the gas velocity is rather constant in the coordinate perpendicular to the flow direction, as the distance between these two positions is also 24 mm.

The ratio of the measured peak centroids of $^{219}Rn^{+}$ ions for the needle source in position I for argon and helium buffer gas was calculated to be 2.94 ± 0.02. This value is reasonably close to the estimate of 3.16, calculated from $\sqrt{A_{Ar}/A_{He}}$, where A_{Ar} and A_{He} are standard atomic weights of argon and helium gas, respectively. This straightforward estimate is based on the fact that the speed of sound $a \sim \sqrt{1/A}$ and, therefore, does not take into account subtle details such as viscous effects that slightly reduce the effective nozzle diameter, the different dynamic viscosity of helium and argon, and minor differences in flow structure e.g., velocity streamlines, between the two gases.

Evacuation time profiles of $^{219}Rn^{+}$ ions for the needle source in helium and argon buffer gas were calculated in the CFD module. Results for the calculated centroids agree well with the experimental data for all positions of the source (see Fig. 8). However, the calculated full widths at half maximum are considerably larger than the measured values for helium buffer gas. This may be caused by erroneous assessment of diffusion in lighter gases and requires more detailed investigation.

3.3. Ion-collector tests

The performance of the ion-collector (IC) electrodes was tested with the ^{223}Ra α-recoil source installed in position I. Measurements were obtained with helium gas at a pressure P_0 of 166 mbar. Mass-separated $^{219}Rn^{+}$ ions were detected as a function of ion-collector voltage at Detector station 2 with the MCP detector, the results are shown in Fig. 9. A suppression to less than 2% of the initial amount was achieved with a voltage of 5 V continuously applied to one of the ICs, while the other was grounded. In order to verify a pulsed operation of the ICs, time profiles of mass-separated $^{219}Rn^{+}$ and $^{20}Ne^{+}$ ions were accumulated with a −20 V amplitude pulse applied to one electrode for 100 ms (see the inset in Fig. 9).

4. In-gas cell laser ionization of tin

In-gas cell laser ionization of stable tin isotopes was performed within argon gas at a pressure P_0 of 100 mbar. The isotopes were produced by resistively heating bronze filaments (91 % copper and 9 % tin, by mass) installed in the gas cell, as shown in Fig. 2. Atomic vapor, produced in this way, was transported by a high-purity argon flow towards the free jet nozzle. Two-step broadband (~ few GHz) laser ionization was used to selectively ionize tin in a collinear geometry, in which both laser beams were transported to the interaction region

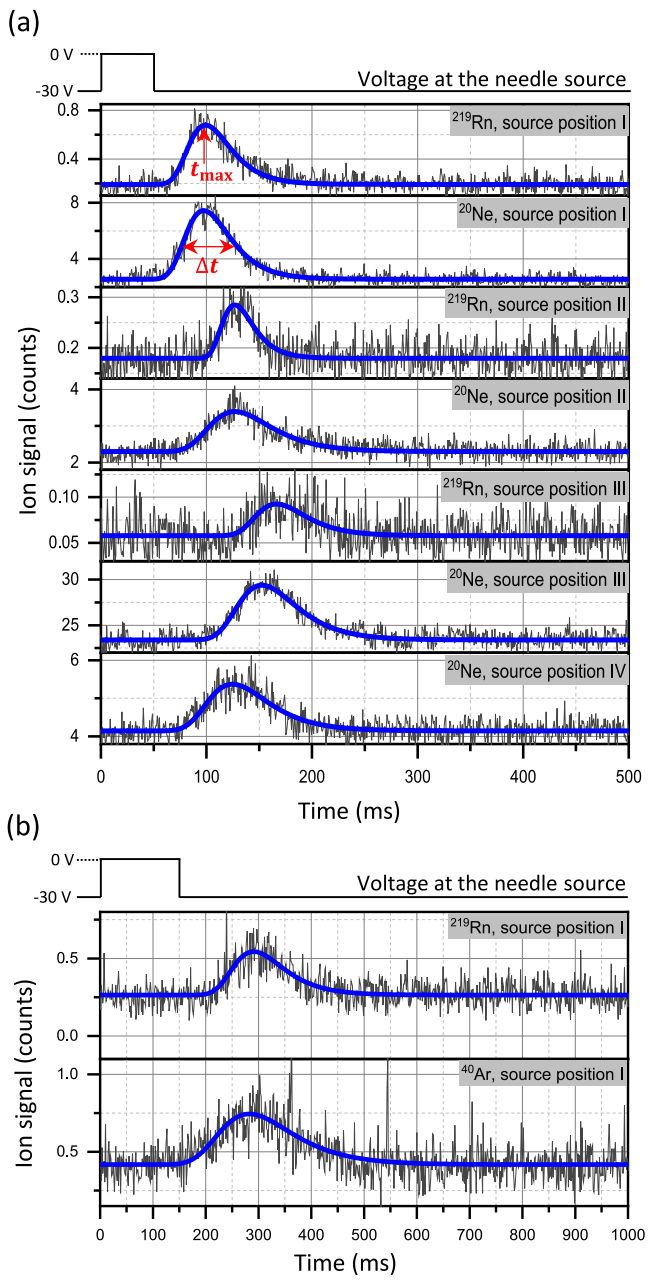

Fig. 7. Evacuation time profiles of the mass-separated $^{219}Rn^+$, $^{20}Ne^+$ and $^{40}Ar^+$ ions. Time profiles of $^{20}Ne^+$ were accumulated within 400 to 700 recording cycles (higher statistics required for the needle source positions with smaller ion counting rates, such as position IV), while for $^{219}Rn^+$ about 4 times longer accumulation was used. Blue solid lines show fitting of measured data (black line) using the Extreme Peak function discussed in the text. (a) Voltage pulsed with a release time of 50 ms applied to the needle source in the gas cell filled with helium buffer gas (P_0 = 200 mbar). The counting rate of $^{20}Ne^+$ ions was about an order of magnitude larger than that of $^{219}Rn^+$. (b) Voltage pulsed with a release time of 150 ms applied to the needle source, using argon as buffer gas (P_0 = 100 mbar). The counting rate of $^{40}Ar^+$ was measured to be approximately the same as that of $^{219}Rn^+$.

through viewport D1 (see Fig. 2). The geometry was chosen primarily due to the ease of optical access via a window on the target chamber. A more versatile optical access that allows for transverse and crossed-beams geometry, as well as for in-gas jet laser ionization will be available on the target chamber of the MARA-LEB facility.

The laser ionization scheme used in these tests is shown in Fig. 10(a), taken from Ref. [29]. The Sn atoms were promoted from the ground state $5s^25p^2\ ^3P_0$ (J = 0) to the intermediate level $5p6s\ ^1P_1$ (J = 1), using frequency-tripled laser light at 254.73 nm (wavelength in vacuum). This transition was easily saturated with the available average laser power of 70 mW measured at the optical table in the FURIOS laboratory. The excited atoms were then ionized via an autoionizing state above the ionization potential, a state that corresponds to the 5p7f configuration, using frequency-doubled laser light at 454.9 nm. By monitoring the count rate of the most abundant isotope, ^{120}Sn, at the MCP of Detector station 2 as a function of the laser power, saturation data can be obtained (see Fig. 10(b)). From a saturation profile fit to the data, a saturation power P_s of 4 mW for the first step was determined. We note that all laser power measurements were made on the optical table, roughly 10 m from the target chamber. Approximately 50% of energy losses are expected for the transport of UV light to the target chamber. The second step transition was not saturated with the available average power of about 400 mW.

By independently blocking the first- and second-step lasers, we verified that the ion signal primarily comes from two-step ionization. The count rate at the MCP dropped to the noise level when the first-step laser was blocked. Blocking only the second-step laser led to the signal decreasing to less than 10 % from its initial value, indicating only a small contribution from any non-resonant ionization processes. Without needing to tune the laser frequency, the mass separator can be used to obtain a mass scan of the laser-ionized tin. As can be seen in Fig. 11, the experimental data is in reasonable agreement with the expected natural isotopic abundances for all isotopes apart from an unexplained underabundance seen at ^{120}Sn. Suppression of laser-ionized ^{120}Sn to around 40 % of its initial value was achieved with 5 V applied to one of the ICs. Further suppression to less than 20 % was achieved with the voltage higher than 20 V. When 5 V were applied to both ICs, the ion signal dropped only to around 60 % due to a cancellation effect of the voltages on the ion beam.

Frequency scans were attempted for both transitions in order to study the effect of the gas pressure on the spectral linewidths and centroids. Unfortunately, the first-step transition was hampered by mode hopping of the broadband laser, making it impossible to do a smooth scan over the desired frequency range. In the future this limitation will be addressed by implementing an injection-locked Ti:Sa laser resonator. Scanning of the second-step transition was however achieved at argon pressure P_0 values ranging from 97 mbar to 203 mbar, with the mass separator tuned to ^{120}Sn. The laser power was reduced to ~1 mW and 300 mW for the first and second steps, respectively, to reduce the effect of power broadening. The results of the frequency scans are shown in Fig. 12. It can be seen that the spectral line broadens as the pressure increases. Notably there is a strong asymmetry in the data. We surmise that the asymmetry arises due to the geometry of the laser ionization. The laser beams pass through viewport D1 (Fig. 2) and are gradually focused towards the free jet nozzle. Ionization is therefore occurring in a collinear geometry both within the gas cell as well as in the volume around the free jet nozzle. The irradiated gas volume contains a convolution of different collisional and Doppler regions. For example, in the nozzle region, the Mach number, velocity and density of gas flow change rapidly over distances as short as a millimeter. This therefore complicates any analysis of the spectral profiles with parametric models to extract pressure broadening and shift coefficients from the data. A non-parametric method of extracting the width of the peaks was used, by determining the range of experimental values that are located above the half maximum of the peak. From this data, an observed broadening of the atomic resonances was found to be on the order of 240 MHz/mbar. In future work, a crossed-beam geometry with a well-defined region of laser-beam overlap is preferable in order to minimize complexities due to convoluting regions of different gas flow.

5. Conclusions

The gas cell designed for the MARA-LEB facility has been characterized at the Accelerator Laboratory of the University of Jyväskylä using

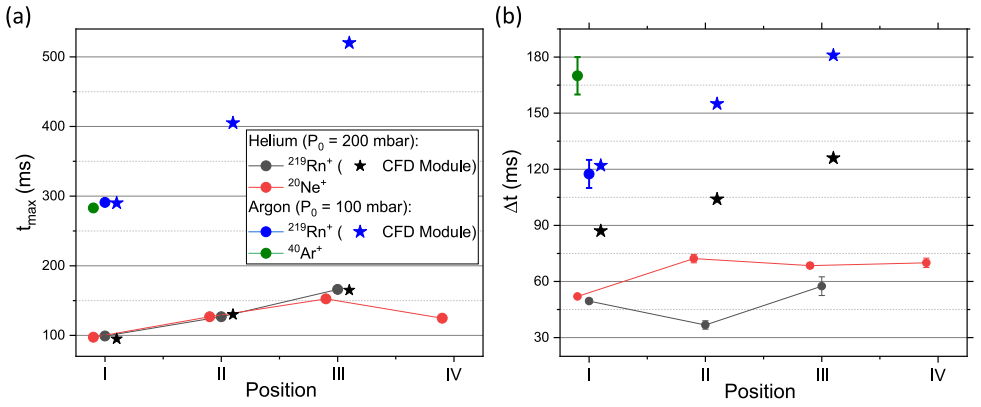

Fig. 8. (a) Peak centroids, t_{max}, and (b) full widths at half maximum, Δt, extracted from $^{219}Rn^+$, $^{20}Ne^+$ and $^{40}Ar^+$ evacuation time profiles, shown in Fig. 7. Overlapping data points are offset around their X-coordinates for clarity.

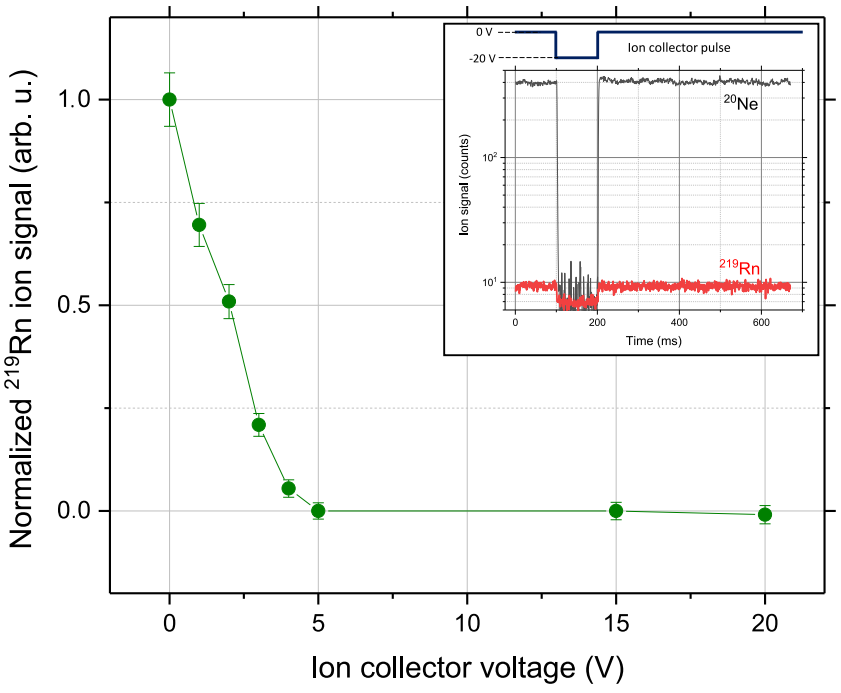

Fig. 9. Normalized signal of $^{219}Rn^+$ ions measured at the MCP detector (Detector station 2) with different voltages applied to one of the ICs. The inset shows time profiles of the mass-separated $^{219}Rn^+$ and $^{20}Ne^+$ ions accumulated in 850 and 130 recording cycles, respectively, each lasting for 0.67 s, with voltage pulses applied to the ion collector (100 ms long and −20 V amplitude). P_0 = 166 mbar in all measurements.

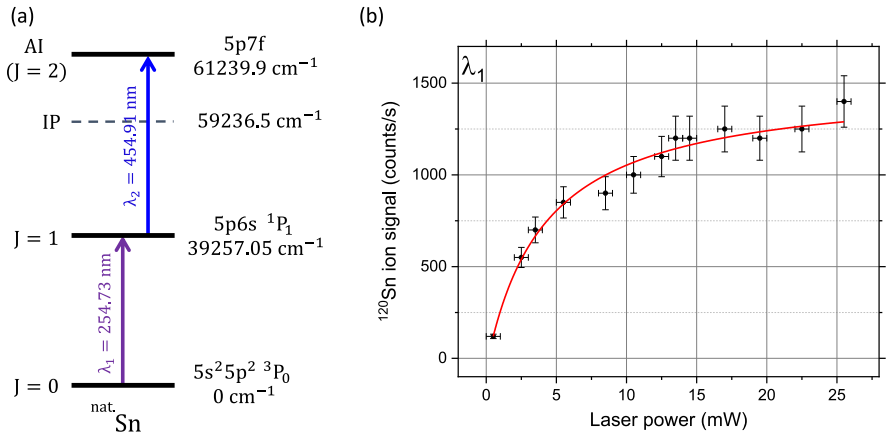

Fig. 10. (a) Two-step laser resonance ionization scheme for tin. (b) Saturation curve for the first-step transition. The laser power (P) was measured in the FURIOS laboratory. The data was fitted (red curve) with a conventional saturation function of the form $I(P) = I_0 + A\frac{P/P_s}{(1+P/P_s)}$, where I_0 is an offset parameter to account for non-resonant photoionization.

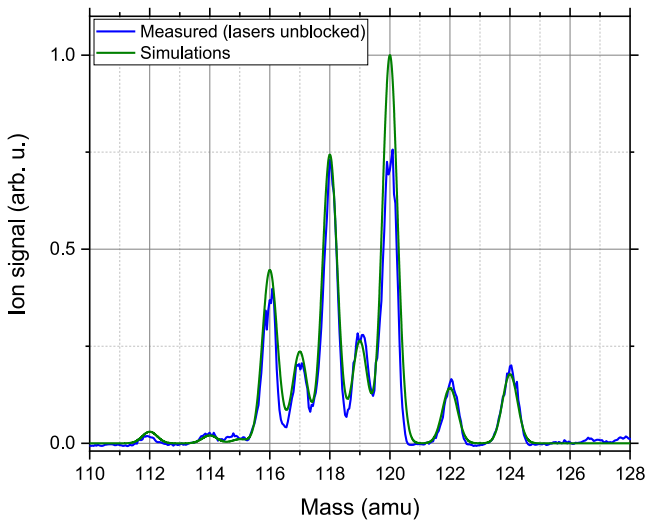

Fig. 11. A scan of the dipole sector magnet of the IGISOL mass separator, showing the resulting laser-ionized stable isotopes of tin (blue line). The green line is a simulated mass scan with the expected isotopic abundances. The experimental data is normalized to the simulated ^{118}Sn peak.

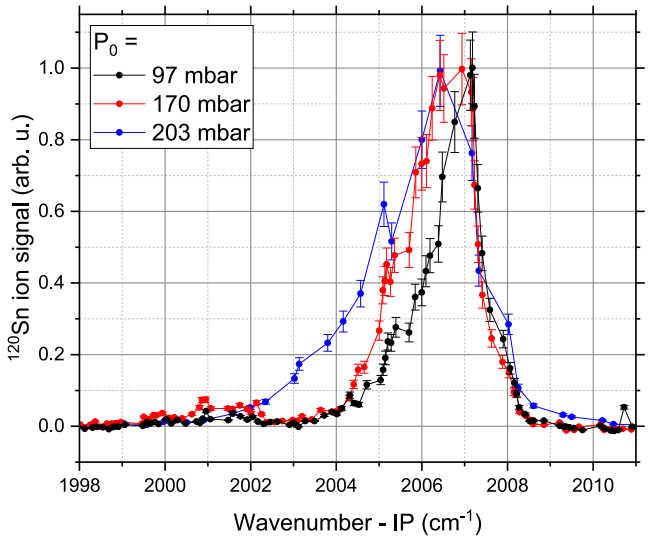

Fig. 12. Normalized ion count rate as a function of the wavenumber of the second-step transition using mass-separated ^{120}Sn, performed at different values of argon pressure P_0. The two-step laser resonance ionization scheme shown in Fig. 10 was used. The horizontal axis indicates the wavenumber (cm^{-1}) with respect to the value of the ionization potential (IP), 59236.5 cm^{-1}.

a ^{223}Ra α-recoil source as well as resonantly-ionized tin isotopes from a heated filament. The ion survival and transport efficiency have been measured at Detector position 1 as a function of recoil source position as well as buffer gas pressure, with a maximum value of ~12.7% obtained for the source located closest to the outflow when helium gas is used. For the same source position and gas type, a corresponding evacuation time of ~100 ms has been measured. An ion survival and transport efficiency of ~8.5% and an evacuation time of ~127 ms were measured for the source positioned in the location at the middle of the entrance window. It has been shown that ionization of the buffer gas and its impurities takes place in the immediate vicinity of the needle tip by the released ^{219}Rn recoils. Numerical calculations of the time profiles of the extracted ions when the recoil source is operated in a pulsed-release mode showed good agreement with the measured data. Suppression of the ion signal of ^{219}Rn was successfully achieved with 5 V applied to one of the ion-collector electrodes, verifying their potential use for improving the selectivity of the in-gas laser resonant ionization process in future experiments.

In-gas-cell laser resonance ionization of stable tin isotopes has been performed and broadening of the atomic resonances with increase of the gas cell pressure was observed for the second step transition. The chosen collinear laser-atom geometry, although successfully used for laser ionization, indicates a strong sensitivity to different regions of gas flow (both Doppler and collisional effects are convoluting), prohibiting extraction of pressure broadening and shift coefficients. This supports a crossed-beams geometry with a well-defined, localized laser ionization volume within the gas cell, to explore the effect of pressure changes on the spectral lineshape. The broadening seen highlights the expected challenges in resolving isotope shifts and hyperfine structure of exotic radioactive tin isotopes in the future, necessitating the requirement of performing resonant laser ionization in the low density and low temperature media of high Mach number gas jets formed downstream from the de Laval nozzles, rather than within the subsonic gas flow regime inside the gas cell.

CRediT authorship contribution statement

A. Zadvornaya: Investigation, Formal analysis, Supervision, Writing – original draft. **J. Romero:** Investigation, Formal analysis. **T. Eronen:** Investigation. **W. Gins:** Investigation, Formal analysis. **A. Kankainen:** Writing – review & editing. **I.D. Moore:** Supervision, Writing – review & editing. **P. Papadakis:** Project administration, Investigation, Writing – review & editing. **I. Pohjalainen:** Investigation. **M. Reponen:** Investigation. **S. Rinta-Antila:** Investigation. **J. Sarén:** Writing – review & editing. **D. Simonovski:** Investigation, Formal analysis, Validation. **J. Uusitalo:** Writing – review & editing.

Declaration of competing interest

The authors declare that they have no known competing financial interests or personal relationships that could have appeared to influence the work reported in this paper.

Data availability

Data will be made available on request

Acknowledgments

This project has received funding from the Academy of Finland under project number 315179 (In-gas-jet laser spectroscopy near the proton dripline). A.Z. acknowledges funding from the European Union's Horizon 2020 research and innovation program under grant agreement No. 771036 (ERC CoG MAIDEN).

References

[1] P. Papadakis, I. Moore, I. Pohjalainen, J. Sarén, J. Uusitalo, Development of a low-energy radioactive ion beam facility for the MARA separator, Hyperfine Interact. 237 (2016) 152, http://dx.doi.org/10.1007/s10751-016-1364-8.

[2] H. Schatz, A. Aprahamian, J. Görres, M. Wiescher, T. Rauscher, J. Rembges, F.-K. Thielemann, B. Pfeiffer, P. Möller, K.-L. Kratz, H. Herndl, B. Brown, H. Rebel, rp-process nucleosynthesis at extreme temperature and density conditions, Phys. Rep. 294 (4) (1998) 167–263, http://dx.doi.org/10.1016/S0370-1573(97)00048-3.

[3] C. Fröhlich, G. Martínez-Pinedo, M. Liebendörfer, F.-K. Thielemann, E. Bravo, W.R. Hix, K. Langanke, N.T. Zinner, Neutrino-induced nucleosynthesis of $A > 64$ nuclei: The νp process, Phys. Rev. Lett. 96 (2006) 142502, http://dx.doi.org/10.1103/PhysRevLett.96.142502.

[4] J. Romero, K. Auranen, M. Block, A.D. Briscoe, T. Eronen, W. Gins, T. Grahn, P.T. Greenlees, A. Illana, R. Julin, H. Joukainen, H. Jutila, J. Khuyagbaatar, J. Krier, M. Leino, J. Louko, M. Luoma, I.D. Moore, P. Mosat, J. Ojala, A. Ortiz-Cortes, J. Pakarinen, P. Papadakis, A.M. Plaza, P. Rahkila, A. Raggio, P. Ruotsalainen, J. Saren, M. Sandzelius, A. Tolosa-Delgado, J. Uusitalo, G. Zimba, Nuclear reaction studies and prospects for the new MARA-LEB facility, Acta Phys. Pol. B Proc. Suppl. 16 (2023) (in press).

[5] P. Papadakis, J. Liimatainen, J. Sarén, I. Moore, T. Eronen, J. Partanen, I. Pohjalainen, S. Rinta-Antila, J. Tuunanen, J. Uusitalo, The MARA-LEB ion transport system, Nucl. Instrum. Methods B 463 (2020) 286–289, http://dx.doi.org/10.1016/j.nimb.2019.05.007.

[6] J. Uusitalo, J. Sarén, J. Partanen, J. Hilton, Mass analyzing recoil apparatus, MARA, Acta Phys. Polon. B 50 (2019) 319, http://dx.doi.org/10.5506/APhysPolB.50.319.

[7] R. Ferrer, et al., In gas laser ionization and spectroscopy experiments at the superconducting separator spectrometer (S^3): Conceptual studies and preliminary design, Nucl. Instrum. Methods B 317 (2013) 570–581, http://dx.doi.org/10.1016/j.nimb.2013.07.028.

[8] Y. Kudryavtsev, P. Creemers, R. Ferrer, C. Granados, L. Gaffney, M. Huyse, E. Mogilevskiy, S. Raeder, S. Sels, P. Van den Bergh, P. Van Duppen, A. Zadvornaya, A new in-gas-laser ionization and spectroscopy laboratory for off-line studies at KU Leuven, Nucl. Instrum. Methods B 376 (2016) 345–352, http://dx.doi.org/10.1016/j.nimb.2016.02.040, Proceedings of the XVIIth International Conference on Electromagnetic Isotope Separators and Related Topics (EMIS2015), Grand Rapids, MI, U.S.A., 11-15 May 2015.

[9] COMSOL Multiphysics, https://www.comsol.com/.

[10] Y. Kudryavtsev, R. Ferrer, M. Huyse, P. Van den Bergh, P. Van Duppen, The in-gas-jet laser ion source: Resonance ionization spectroscopy of radioactive atoms in supersonic gas jets, Nucl. Instrum. Methods B 297 (2013) 7–22, http://dx.doi.org/10.1016/j.nimb.2012.12.008.

[11] A. Zadvornaya, et al., Characterization of supersonic gas jets for high-resolution laser ionization spectroscopy of heavy elements, Phys. Rev. X 8 (2018) 041008, http://dx.doi.org/10.1103/PhysRevX.8.041008.

[12] J. Äystö, A. Jokinen, T. Eronen, A. Kankainen, I. Moore, H. Penttilä (Eds.), Three Decades of Research Using IGISOL Technique at the University of Jyväskylä, Springer, International, 2014.

[13] J. Huikari, P. Dendooven, A. Jokinen, A. Nieminen, H. Penttilä, K. Peräjärvi, A. Popov, S. Rinta-Antila, J. Äystö, Production of neutron deficient rare isotope beams at IGISOL: on-line and off-line studies, Nucl. Instrum. Methods B 222 (3) (2004) 632–652, http://dx.doi.org/10.1016/j.nimb.2004.04.164.

[14] J. Eberz, U. Dinger, G. Huber, H. Lochmann, R. Menges, G. Ulm, R. Kirchner, O. Klepper, T. Kühl, D. Marx, Nuclear spins, moments and charge radii of $^{108-111}$Sn, Z. Phys. A 326 (1987) 121–129, http://dx.doi.org/10.1007/BF01283586.

[15] P. Karvonen, I.D. Moore, T. Sonoda, T. Kessler, H. Penttilä, K. Peräjärvi, P. Ronkanen, J. Äystö, A sextupole ion beam guide to improve the efficiency and beam quality at IGISOL, Nucl. Instrum. Methods B 266 (21) (2008) 4794–4807, http://dx.doi.org/10.1016/j.nimb.2008.07.022.

[16] R.J. van Sonsbeek, Ronald Cooper, R.N. Bhave, Pulse radiolysis studies of ion–electron recombination in helium. Pressure and temperature effects, J. Chem. Phys. 97 (1992) http://dx.doi.org/10.1063/1.463167, 1800–.

[17] Ronald Cooper, R.J. van Sonsbeek, R.N. Bhave, Pulse radiolysis studies of ion-electron recombination in gaseous argon, J. Chem. Phys. 98 (1993) http://dx.doi.org/10.1063/1.464631, 383–.

[18] M. Facina, B. Bruyneel, S. Dean, J. Gentens, M. Huyse, Y. Kudryavtsev, P. Van den Bergh, P. Van Duppen, A gas cell for thermalizing, storing and transporting radioactive ions and atoms. Part II: On-line studies with a laser ion source, Nucl. Instrum. Methods B 226 (3) (2004) 401–418, http://dx.doi.org/10.1016/j.nimb.2004.06.031.

[19] I. Pohjalainen, I.D. Moore, T. Eronen, A. Jokinen, H. Penttilä, S. Rinta-Antila, Gas purification studies at IGISOL-4, Hyperfine Interact. 227 (2014) 169–180, http://dx.doi.org/10.1007/s10751-013-1006-3.

[20] M. Reponen, I.D. Moore, I. Pohjalainen, V. Sonnenschein, A. Jokinen, The FURIOS laser ion source at IGISOL-4, Nucl. Instrum. Methods B 317 (2013) 422–425, http://dx.doi.org/10.1016/j.nimb.2013.05.061, XVIth International Conference on ElectroMagnetic Isotope Separators and Techniques Related to their Applications, December 2–7, 2012 at Matsue, Japan.

[21] V. Sonnenschein, I.D. Moore, S. Raeder, M. Reponen, H. Tomita, K. Wendt, Characterization of a pulsed injection-locked Ti:sapphire laser and its application to high resolution resonance ionization spectroscopy of copper, Laser Phys. 27 (8) (2017) 085701, http://dx.doi.org/10.1088/1555-6611/aa7834.

[22] M. Reponen, Resonance Laser Ionization Developments for IGISOL-4 (Ph.D. thesis), 2012.

[23] P.J. Gardner, P. Pang, S.R. Preston, Binary gaseous diffusion coefficients of mercury and of zinc in hydrogen, helium, argon, nitrogen, and carbon dioxide, J. Chem. Eng. Data 36 (0021–9568) (1991) http://dx.doi.org/10.1021/je00003a003.

[24] Y. Kudryavtsev, B. Bruyneel, M. Huyse, J. Gentens, P. Van den Bergh, P. Van Duppen, L. Vermeeren, A gas cell for thermalizing, storing and transporting radioactive ions and atoms. Part I: Off-line studies with a laser ion source, Nucl. Instrum. Methods B 179 (3) (2001) 412–435, http://dx.doi.org/10.1016/S0168-583X(01)00575-4.

[25] P. Dendooven, S. Purushothaman, K. Gloos, On a cryogenic noble gas ion catcher, Nucl. Instrum. Methods A 558 (2) (2006) 580–583, http://dx.doi.org/10.1016/j.nima.2005.12.201.

[26] W. Plaß, T. Dickel, S. Purushothaman, P. Dendooven, H. Geissel, J. Ebert, E. Haettner, C. Jesch, M. Ranjan, M. Reiter, H. Weick, F. Amjad, S. Ayet, M. Diwisch, A. Estrade, F. Farinon, F. Greiner, N. Kalantar-Nayestanaki, R. Knöbel, J. Kurcewicz, J. Lang, I. Moore, I. Mukha, C. Nociforo, M. Petrick, M. Pfützner, S. Pietri, A. Prochazka, A.-K. Rink, S. Rinta-Antila, D. Schäfer, C. Scheidenberger, M. Takechi, Y. Tanaka, J. Winfield, M. Yavor, The FRS Ion Catcher – A facility for high-precision experiments with stopped projectile and fission fragments, Nucl. Instrum. Methods B 317 (2013) 457–462, http://dx.doi.org/10.1016/j.nimb.2013.07.063.

[27] OriginPro, Version 2017, OriginLab Corporation, Northampton, MA, USA, https://www.originlab.com/.

[28] D. Simonovski, Offline Tests with the Fission Ion Guide and MARA-LEB Gas Cell at the IGISOL-4 Facility, Tech. Rep., University of Jyväskylä.

[29] A. Nadeem, S.A. Bhatti, N. Ahmad, M.A. Baig, Two-step laser excitation of $5p_{3/2}np$, nf $J = 1$ and 2 autoionizing Rydberg levels of tin, J. Phys. B: At. Mol. Opt. Phys. 33 (18) (2000) 3729, http://dx.doi.org/10.1088/0953-4075/33/18/321.